Electronic Supplementary Material (ESI) for Sustainable Energy & Fuels.

Effects of Pt Metal Loading on Atomic Restructure and Oxygen Reduction Reaction Performance of Pt-Cluster Decorated Cu@Pd Electrocatalysts

Authors: Dinesh Bhalothia,[a,b] Cheng-Yang Lin,[a] Che Yan,[b] Ya-Tang Yang,[a*] and Tsan-Yao Chen[b,c,d,e*]

Affiliations:

[a.] Institute of Electronics Engineering, National Tsing Hua University, Hsinchu 30013, Taiwan

[b.] Department of Engineering and System Science, National Tsing Hua University, Hsinchu 30013, Taiwan

[c.] Institute of Nuclear Engineering and Science, National Tsing Hua University, Hsinchu 30013, Taiwan

[d.] Hierarchical Green-Energy Materials (Hi-GEM) Research Centre, National Cheng Kung University, Tainan 70101, Taiwan

[e.] Higher Education Sprout Project, Competitive Research Team, National Tsing Hua University, Hsinchu 30013, Taiwan

Corresponding Author:

Tsan-Yao Chen

Email: chencaeser@gmail.com

Tel: +886-3-5715131 # 34271

FAX: +885-3-5720724

1. HRTEM image of Cu@Pd NC.

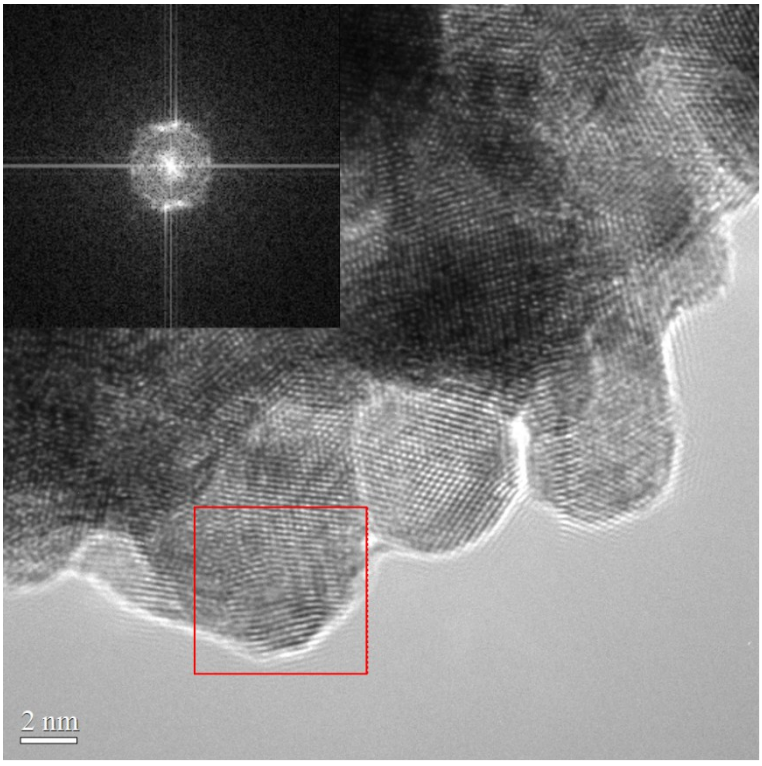

Figure S1. HRTEM images of Cu@Pd NC.

2. HRTEM analysis of control sample (Pt-CNT).

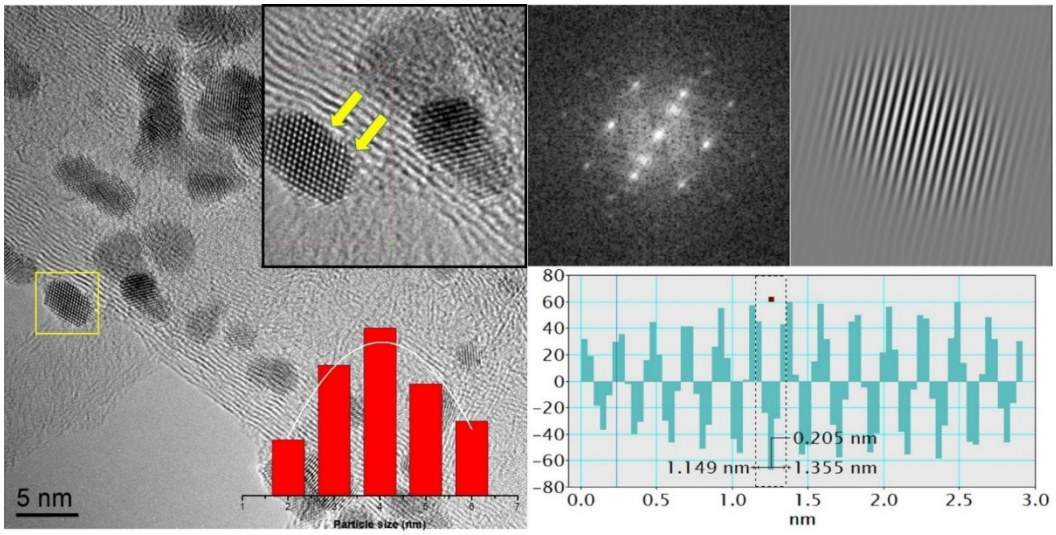

Figure S2. HRTEM image Pt-CNT. d-spacing values is calculated by using Inverse Fourier Transformed (IFT) images and their corresponding line histograms (insets). Fourier transformation pattern of selected area in HRTEM image is shown in corner.

3. Structural interpretation for crystal growth of control samples via comparative XRD spectra analysis.

As depicted in **Figure S3a**, peaks X_1 and X_2 refers to diffraction signals from (111) and (200) facets of metallic Pt phase in Pt-CNT crystal. Whereas, for Pd-CNT, the asymmetry peak profiles are attributed to PdO phase. Meanwhile, in case of Cu-CNT XRD spectrum, the three sharp peaks posited at 16.125^o, 18.639^o, and 19.017^o refers to diffraction signals of Cu_2O (111), Cu_2O (110), and CuO (111). On the other hand, for Pd@Pt, compared to that of Pd-CNT, larger extent of peak upshift at X_2 reveals the higher extent of Pd-to-Pt intermix at (200) facets. Such an uneven intermix is due to easy intercalation of Pt atoms in opened surfaces. Meanwhile, broadened peak with increased background diffusion scattering hump at peak region are caused by increasing surface roughness of NC. Such phenomena explain the intercalation of atomic Pt clusters into near-surface region of Pd@Pt NC.

Figure S3b represents comparative XRD patterns of CuPP-03 NC with control samples. Accordingly, substantial upshift of (111) and (200) peaks indicate the strong lattice compression in CuPP-03 NC. For Cu@Pt, significant suppression on peak intensities indicate the strong confinement effect on Cu crystal growth by adjacent to Pt crystal. The splitting of main diffraction line indicates the formation of Cu_3Pt alloy. In case of Cu@Pd, substantially decreased peak intensity at 16.2^o (as compared to Cu-CNT) illustrating the suppression of Cu_2O growth by a subsequent reduction of Pd crystal in Cu NP surface of Cu@Pd.

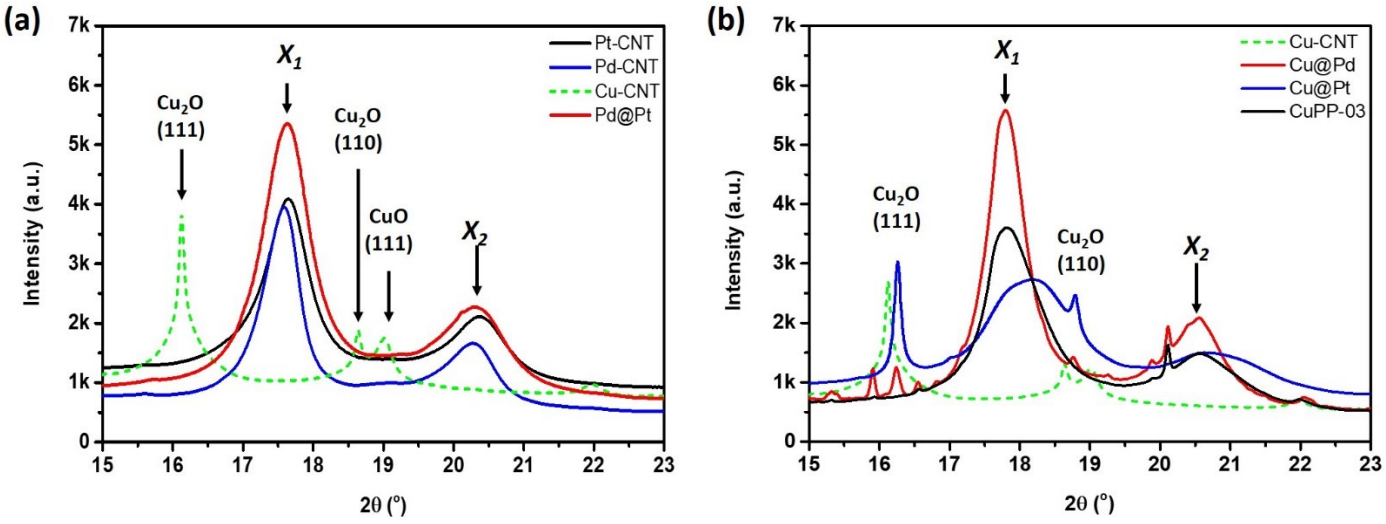

Figure S3. XRD patterns of (a) Pt-CNT, Pd-CNT and Cu-CNT compared with Pd@Pt and (b) control samples compared with CuPP-03 NC.

4. X-ray absorption spectroscopy analysis at Cu k-edge of experimental CuPP NCs series and control samples.

X-ray absorption spectroscopy (XAS) has proven to be an outstanding structural tool by allowing the determination of the local environment around a selected atomic species in a great variety of systems. In order to elucidate the electronic structure of Cu-core crystal and to get further evidence of charge relocations XAS analysis has been done at Cu K-edge. As shown in **Figure S4**, for CuPP-03, highest intensity of pre-edge peak (X) nearly similar to the Cu-foil, refers that Cu gets restructured in this case and gain its metallic phase. Such a hypothesis is further confirmed by lowest white line intensity for CuPP-03. This suggests that lowest amount of oxygen absorption took place in this case.

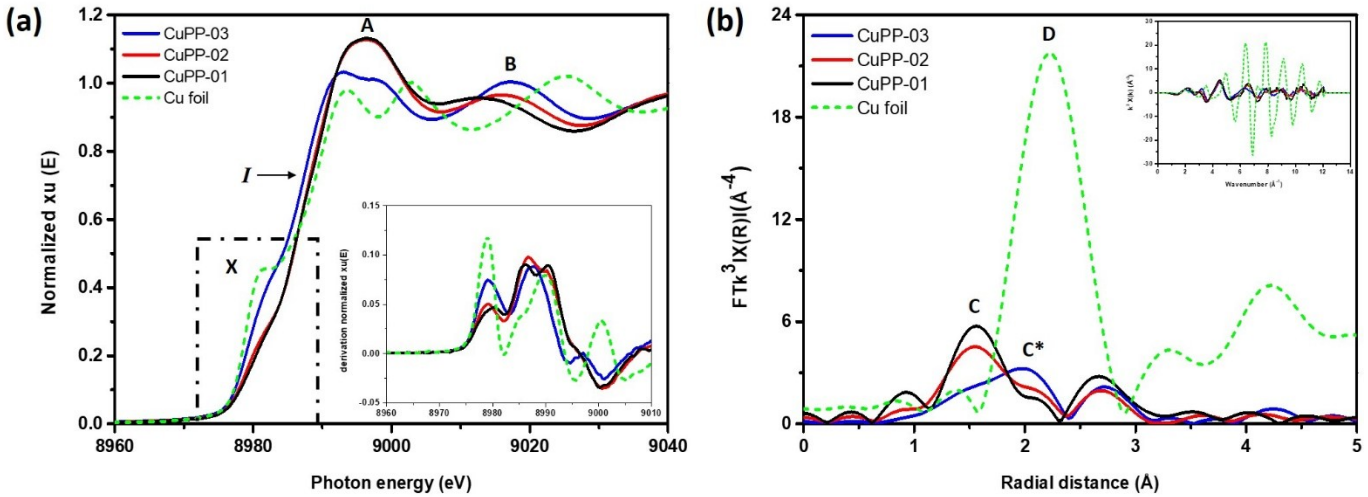

Figure S4. Cu K-edge X-ray absorption spectroscopy of experimental NCs in (a) X-ray absorption near-edge structure (XANES) and (b) extended X-ray absorption fine structure regions.

As depicted in **Figure. S5**, similar position of reflection points (*I*) for Pt-CNT and Pt foil suggests identical chemical state of the two sample.

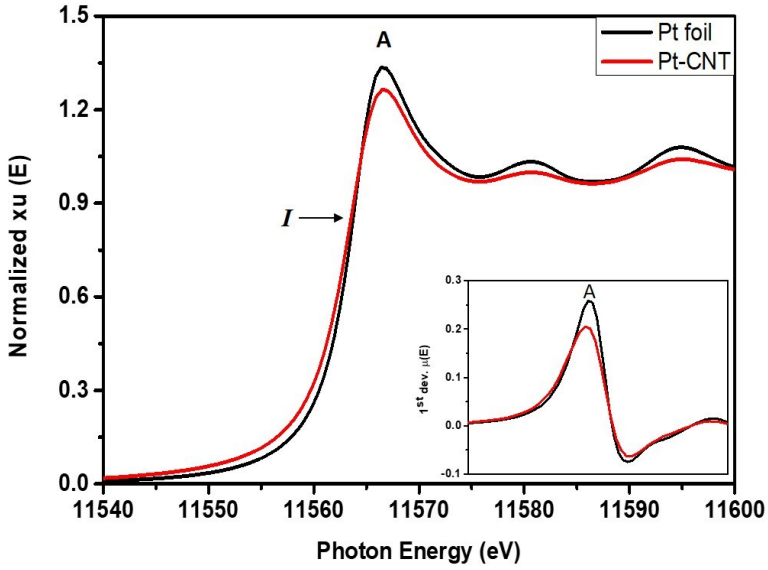

Figure S5. Pt L3-edge XANES spectra of Pt-CNT and standard Pt foil.

5. XAS data collection, normalization, and model analysis: -

The heteroatomic intermixes and the unfilled valence orbital states (unfilled d states) of the electrochemical active atoms (Pt) of CuPP were determined by X-ray absorption spectroscopy (XAS). All the XAS spectra were recorded at the wiggler beam line of BL-17C and 07A (for Pt L_3-edge, E_0 = 11564 eV and Cu *K*-edge, E_0 = 8979 eV), and the superconducting wavelength shifter beam line of BL-01C1 (for Pd *K*-edge, E_0 = 24350 eV) of NSRRC using florescence mode X-ray detection by a Lytle detector.[35] Upon data collection, the appropriate filters (Ni, Ga, and Mo respectively for Cu *K*, Pt L_3, and Pd *K*-edges) were placed in front of the detector to eliminate the scattering background. The incident and transmitting X-ray through the reference sample was recorded after each XAS scan to obtain the reference spectrum for calibrating the energy of the incident X-ray.

The XAS data including the XANES and the EXAFS oscillations ($\chi(k)$), where *k* is the photoelectron wave number, were extracted and normalized according to the standard procedures of Athena program (with the code of AUTOBK algorithm 2.93) in the IFEFFIT package (version 1.2.10)[1-4]. Using a Hanning window function forward Fourier transformation (FFT) was performed on the EXAFS region of normalized XAS spectra with the selected *k* ranges for the Pt L_3 (from 3.25 to 12.1 $Å^{-1}$) and Pd *K*-edges (from 2.85 to 12.50 $Å^{-1}$) to generate the radial structure functions (RSF) in the radial space ranging from 0 to 5.0 Å.

To conduct a XAS model analysis (calculation), the reference structural information of standard Pt, and Pd crystals (obtained from the Inorganic Crystal Structure Database (ICSD) and WebAtoms Database) was implemented in FEFF6.20 program[5] in the IFEFFIT package (version 1.2.10)[1-3] to generate theoretical bond paths of Pt-Pt, Pt-Pd, and Pt-Cu for Pt L_3-edge (while, Pd-Pd, Pd-Pt, and Pd-Cu for Pd K-edge) analysis. The model of Pt L_3-edge XAS fitting was based on the cadre of Pt FCC crystal (with a $Fm\bar{3}m$ symmetry), where the number of neighboring atoms in the nearest shell (N_{Pt-N}) is 12 at the interatomic distance (R_{Pt-N}) of 2.772 Å. The bond path of heteroatoms was generated by substituting Pt with Cu and Pd in the first coordination shell of the lattice model. For the Pd *K*-edge model fitting, the atomic structure model was generated by using the framework of Pd FCC crystal (with a $Fm\bar{3}m$ symmetry), where the number of neighboring atoms in the first

two nearest shells (N_{Pd-N1}) is 12 at the interatomic distance (R_{Pd-N}) around 2.672 Å.

The obtained RSF function was analyzed using EXAFS simulation (Artemis kits) with appropriate models (the scattering paths of Pt-Pt, Pt-Pd, and Pt-Cu bonding pairs) to investigate the local structural parameters (including the structural parameters of interatomic bond distance (R_{ij}), phase shifts (Φ_{ij}), coordination numbers (N_j), amplitude reduction factor (S_i^2), effective wave backscattering amplitude ($F_j(k)$), and Debye-Waller factor (σ_j^2)) around X-ray excited atoms in IFEFFIT program with EFEE6.01 code. To simplify the EXAFS fitting, the values of S_i^2 of Pt and Cu atoms were fixed at 0.83 which was in good agreement with the theoretical estimation and can be used for different samples with central atoms in a similar chemical state (valence, coordination). Only single scattering paths were considered in fitting the experimental XAS data to prevent unexpected analytical errors (which may be due to the background noises or the multiple scattering effects from the higher order shells). The model simulation of XAS fitting with metal substitution was conducted by incorporating appropriate constrains in a single coordination shell. To evaluate the local structural information around X-ray excited atoms, we adopted independent iterations to avoid the unexpected errors of direct correlation between structural parameters. The $k^3\chi(k)$ were fitted with all the possible scattering paths for the corresponding FT peaks, where structural parameters of σ_j^2, N_j, and the R_{ij} were treated as adjustable parameters[12]. The atomic intermixes for Pt (χ_{Pt-Pt}), Pd (χ_{Pt-Pd}), and Cu (χ_{Pt-Cu}) to Pt atoms are determined to be CN_{Pt-Pt}, CN_{Pt-Pd}, and CN_{Pt-Cu} divided by $CN_{Pt-total}$; where CN_{Pt-Pt}, CN_{Pt-Pd}, CN_{Pt-Cu}, and $CN_{Pt-total}$ respectively refer to the coordination number of Pd, Cu, and total neighboring atoms around Pt atoms. For the case of Pd, χ_{Pd-Pd}, χ_{Pd-Pt}, and χ_{Pd-Cu} are determined to be CN_{Pd-Pd}, CN_{Pd-Pt}, and CN_{Pd-Cu} divided by $CN_{Pd-total}$.

6. Electrochemical performances of CuPP nanocatalysts compared with Cu@Pd and commercial Pt catalysts (JM-Pt/C)

Table S1. Electrochemical performances of CuPP nanocatalysts compared with Cu@Pd and commercial Pt catalysts (JM-Pt/C)

Sample	N	ECSA $cm^2\ mg_{Pt+Pd}^{-1}$	E_{onset} V vs RHE	$J_{K0.85}$ $mA\ cm^{-2}$	$S.A._{0.85}$ $mA\ cm^{-2}$	$M.A._{0.85}$ $mA\ mg_{Pt}^{-1}$
CuPP-03	3.9	546.7	0.925	21.6	0.265	408.0
CuPP-02	3.9	632.0	0.916	18.4	0.211	498.0
CuPP-01	3.8	998.0	0.909	12.4	0.099	639.4
Cu@Pd	3.8	471.4	0.870	1.6	0.031	N.A.
J.M.-Pt/C	4.0	257.0	0.915	5.3	0.261	67.0

7. Electrochemical performances of commercial Pt catalysts (JM-Pt/C) before and after 31000 ADT cycles

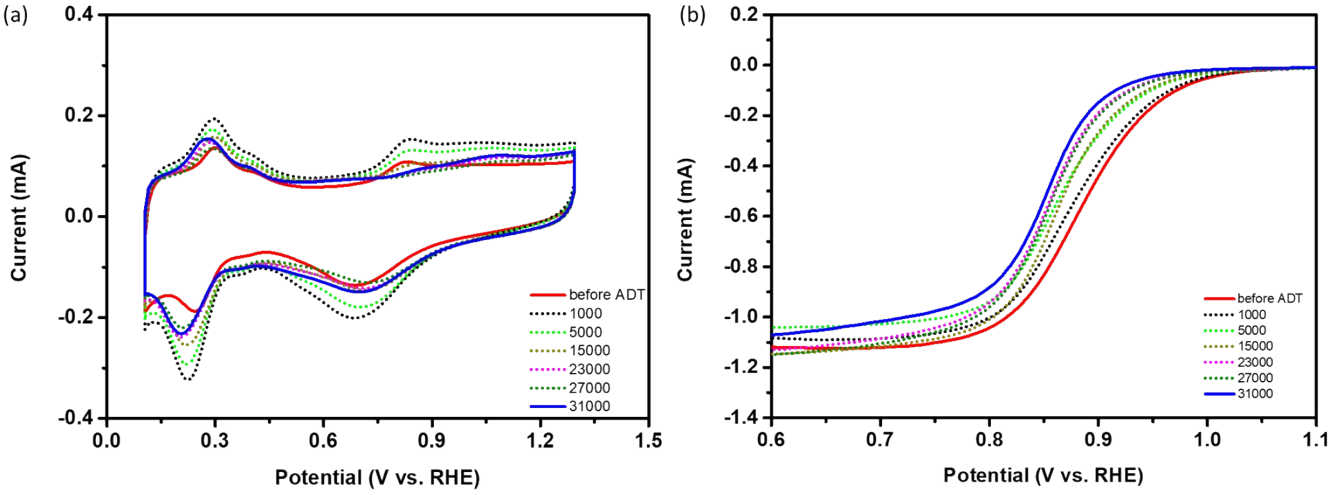

Figure S6. Electrochemical performances of commercial Pt catalysts (JM-Pt/C) before and after 31000 ADT cycles

Table S2. Actual weight of constituent elements in CuPP experimental nanocatalysts during synthesis.

Sample	CNT (gm)	Cu (gm)	Pd (gm)	Pt (gm)
CuPP-01	0.025	0.0075	0.013	2.30E-03
CuPP-02	0.025	0.0075	0.013	4.60E-03
CuPP-03	0.025	0.0075	0.013	6.91E-03

*Unit is in grams